THz conductivities of indium-tin-oxide nanowhiskers as a graded-refractive-index structure

Chan-Shan Yang,[1] Chia-Hua Chang,[2] Mao-Hsiang Lin,[1] Peichen Yu,[2] Osamu Wada,[1,3,4] and Ci-Ling Pan[1,5,*]

[1]*Department of Physics, National Tsing Hua University, Hsinchu, 30013 Taiwan*
[2]*Department of Photonics and Institute of Electro-Optical Engineering, National Chiao Tung University, Hsinchu, 30010 Taiwan*
[3]*Center for Collaborative Research and Technology Development, Kobe University, Kobe 657-8501, Japan*
[4]*Department of Electronics and Electrical Engineering, The University of Sheffield, Sheffield S1 3JD, UK*
[5]*Frontier Research Center on Fundamental and Applied Science of Matters, National Tsing Hua University, Hsinchu, 30013 Taiwan*
[*]*clpan@phys.nthu.edu.tw*

Abstract: Indium-tin-oxide (ITO) nanowhiskers with attractive electrical and anti-reflection properties were prepared by the glancing-angle electron-beam evaporation technique. Structural and crystalline properties of such nanostructures were examined by scanning transmission electron microscopy and X-ray diffraction. Their frequency-dependent complex conductivities, refractive indices and absorption coefficients have been characterized with terahertz time-domain spectroscopy (THz-TDS), in which the nanowhiskers were considered as a graded-refractive-index (GRIN) structure instead of the usual thin film model. The electrical properties of ITO GRIN structures are analyzed and fitted well with Drude-Smith model in the 0.2~2.0 THz band. Our results indicate that the ITO nanowhiskers and its bottom layer atop the substrate exhibit longer carrier scattering times than ITO thin films. This signifies that ITO nanowhiskers have an excellent crystallinity with large grain size, consistent with X-ray data. Besides, we show a strong backscattering effect and fully carrier localization in the ITO nanowhiskers.

OCIS codes: (040.2235) Far infrared or terahertz; (120.4290) Nondestructive testing; (120.4530) Optical constants; (160.4236) Nanomaterials; (220.4241) Nanostructure fabrication; (260.2065) Effective medium theory; (290.1350) Backscattering; (300.6270) Spectroscopy, far infrared; (300.6495) Spectroscopy, terahertz.

References and links

1. G. Xu, Z. Liu, J. Ma, B. Liu, S.-T. Ho, L. Wang, P. Zhu, T. J. Marks, J. Luo, and A. K. Y. Jen, "Organic electro-optic modulator using transparent conducting oxides as electrodes," Opt. Express **13**(19), 7380–7385 (2005).
2. G. J. Exarhos and X.-D. Zhou, "Discovery-based design of transparent conducting oxide films," Thin Solid Films **515**(18), 7025–7052 (2007).
3. H. Li, N. Wang, and X. Liu, "Optical and electrical properties of vanadium doped Indium oxide thin films," Opt. Express **16**(1), 194–199 (2008).
4. F. Yi, F. Ou, B. Liu, Y. Huang, S.-T. Ho, Y. Wang, J. Liu, T. J. Marks, S. Huang, J. Luo, A. K.-Y. Jen, R. Dinu, and D. Jin, "Electro-optic modulator with exceptional power-size performance enabled by transparent conducting electrodes," Opt. Express **18**(7), 6779–6796 (2010).
5. C. K. Choi, K. D. Kihm, and A. E. English, "Optoelectric biosensor using indium-tin-oxide electrodes," Opt. Lett. **32**(11), 1405–1407 (2007).
6. Ö. Şenlik, H. Y. Cheong, and T. Yoshie, "Design of subwavelength-size, indium tin oxide (ITO)-clad optical disk cavities with quality-factors exceeding 10^4," Opt. Express **19**(23), 23469–23474 (2011).
7. J. W. Leem and J. S. Yu, "Glancing angle deposited ITO films for efficiency enhancement of a-Si:H/μc-Si:H tandem thin film solar cells," Opt. Express **19**(S3 Suppl 3), A258–A268 (2011).

#165387 - $15.00 USD Received 23 Mar 2012; revised 25 Apr 2012; accepted 30 Apr 2012; published 10 May 2012

8. S. H. Lee and N. Y. Ha, "Nanostructured indium-tin-oxide films fabricated by all-solution processing for functional transparent electrodes," Opt. Express **19**(22), 21803–21808 (2011).
9. W.-Y. Chang, H.-J. Lin, and J.-S. Chang, "Optical panel with full multitouch using patterned indium tin oxide," Opt. Lett. **36**(6), 894–896 (2011).
10. Y.-J. Liu, C.-C. Huang, T.-Y. Chen, C.-S. Hsu, J.-K. Liou, T.-Y. Tsai, and W.-C. Liu, "Implementation of an indium-tin-oxide (ITO) direct-ohmic contact structure on a GaN-based light emitting diode," Opt. Express **19**(15), 14662–14670 (2011).
11. Z. R. Dai, Z. W. Pan, and Z. L. Wang, "Novel nanostructures of functional oxides synthesized by thermal evaporation," Adv. Funct. Mater. **13**(1), 9–24 (2003).
12. J. K. Kim, S. Chhajed, M. F. Schubert, E. F. Schubert, A. J. Fischer, M. H. Crawford, J. Cho, H. Kim, and C. Sone, "Light-extraction enhancement of GaInN light-emitting diodes by graded-refractive-index indium tin oxide anti-reflection contact," Adv. Mater. (Deerfield Beach Fla.) **20**(4), 801–804 (2008).
13. P. Yu, C.-H. Chang, C.-H. Chiu, C.-S. Yang, J.-C. Yu, H.-C. Kuo, S.-H. Hsu, and Y.-C. Chang, "Efficiency enhancement of GaAs photovoltaics employing antireflective indium tin oxide nanocolumns," Adv. Mater. (Deerfield Beach Fla.) **21**(16), 1618–1621 (2009).
14. C.-H. Chang, M.-H. Hsu, P.-C. Tseng, P. Yu, W.-L. Chang, W.-C. Sun, and W.-C. Hsu, "Enhanced angular characteristics of indium tin oxide nanowhisker-coated silicon solar cells," Opt. Express **19**(S3 Suppl 3), A219–A224 (2011).
15. C. H. Chang, P. Yu, and C. S. Yang, "Broadband and omnidirectional antireflection from conductive indium-tin-oxide nanocolumns prepared by glancing-angle deposition with nitrogen," Appl. Phys. Lett. **94**(5), 051114 (2009).
16. S.-P. Chiu, H.-F. Chung, Y.-H. Lin, J.-J. Kai, F.-R. Chen, and J.-J. Lin, "Four-probe electrical-transport measurements on single indium tin oxide nanowires between 1.5 and 300 K," Nanotechnology **20**(10), 105203 (2009).
17. Q. Wan, Z. T. Song, S. L. Feng, and T. H. Wang, "Single-crystalline tin-ddoped indium oxide whiskers: Synthesis and characterization," Appl. Phys. Lett. **85**(20), 4759–4761 (2004).
18. T. Bauer, J. S. Kolb, T. Löffler, E. Mohler, H. G. Roskos, and U. C. Pernisz, "Indium-tin-oxide-coated glass as dichroic mirror for far-infrared electromagnetic radiation," J. Appl. Phys. **92**(4), 2210–2212 (2002).
19. K. Takase, T. Ohkubo, F. Sawada, D. Nagayama, J. Kitagawa, and Y. Kadoya, "Propagation characteristics of terahertz electrical signals on micro-strip lines made of optically transparent conductors," Jpn. J. Appl. Phys. **44**(32), L1011–L1014 (2005).
20. D. G. Cooke and P. U. Jepsen, "Optical modulation of terahertz pulses in a parallel plate waveguide," Opt. Express **16**(19), 15123–15129 (2008).
21. J. Kröll, J. Darmo, and K. Unterrainer, "Metallic wave-impedance matching layers for broadband terahertz optical systems," Opt. Express **15**(11), 6552–6560 (2007).
22. S. H. Brewer and S. Franzen, "Indium tin oxide plasma frequency dependence on sheet resistance and surface adlayers determined by reflectance FTIR spectroscopy," J. Phys. Chem. B **106**(50), 12986–12992 (2002).
23. C.-W. Chen, Y.-C. Lin, C.-H. Chang, P. Yu, J.-M. Shieh, and C.-L. Pan, "Frequency-dependent complex conductivities and dielectric responses of indium tin oxide thin films from the visible to the far-infrared," IEEE J. Quantum Electron. **46**(12), 1746–1754 (2010).
24. C.-W. Chen, T.-T. Tang, S.-H. Lin, J. Y. Huang, C.-S. Chang, P.-K. Chung, S.-T. Yen, and C.-L. Pan, "Optical properties and potential applications of ε-GaSe at terahertz frequencies," J. Opt. Soc. Am. B **26**(9), A58–A65 (2009).
25. X. H. Zhang, H. C. Guo, A. M. Yong, J. D. Ye, S. T. Tan, and X. W. Sun, "Terahertz dielectric response and optical conductivity of n-type single-crystal ZnO epilayers grown by metalorganic chemical vapor deposition," J. Appl. Phys. **107**(3), 033101 (2010).
26. M. Walther, D. G. Cooke, C. Sherstan, M. Hajar, M. R. Freeman, and F. A. Hegmann, "Terahertz conductivity of thin gold films at the metal-insulator percolation transition," Phys. Rev. B **76**(12), 125408 (2007).
27. J. B. Baxter and C. A. Schmuttenmaer, "Conductivity of ZnO nanowires, nanoparticles, and thin films using time-resolved terahertz spectroscopy," J. Phys. Chem. B **110**(50), 25229–25239 (2006).
28. S. A. Jewell, E. Hendry, T. H. Isaac, and J. R. Sambles, "Tunable Fabry-Perot etalon for terahertz radiation," New J. Phys. **10**(3), 033012 (2008).
29. N. V. Smith, "Classical generalization of the Drude formula for the optical conductivity," Phys. Rev. B **64**(15), 155106 (2001).
30. C.-H. Chang, P. Yu, M.-H. Hsu, P.-C. Tseng, W.-L. Chang, W.-C. Sun, W.-C. Hsu, S.-H. Hsu, and Y.-C. Chang, "Combined micro- and nano-scale surface textures for enhanced near-infrared light harvesting in silicon photovoltaics," Nanotechnology **22**(9), 095201 (2011).
31. S. Takaki, Y. Aoshima, and R. Satoh, "Growth mechanism of indium tin oxide whiskers prepared by sputtering," Jpn. J. Appl. Phys. **46**(6A), 3537–3544 (2007).
32. W. J. Heward and D. J. Swenson, "Phase equilibria in the pseudo-binary In_2O_3-SnO_2 system," J. Mater. Sci. **42**(17), 7135–7140 (2007).
33. X. S. Peng, G. W. Meng, X. F. Wang, Y. W. Wang, J. Zhang, X. Liu, and L. D. Zhang, "Synthesis of oxygen-deficient indium-tin-oxide (ITO) nanofibers," Chem. Mater. **14**(11), 4490–4493 (2002).
34. Y. Q. Chen, J. Jiang, B. Wang, and J. G. Hou, "Synthesis of tin-doped indium oxide nanowires by self-catalytic VLS growth," J. Phys. D Appl. Phys. **37**(23), 3319–3322 (2004).

#165387 - $15.00 USD Received 23 Mar 2012; revised 25 Apr 2012; accepted 30 Apr 2012; published 10 May 2012

35. Y. Wu and P. Yang, "Direct observation of vapor-liquid-solid nanowire growth," J. Am. Chem. Soc. **123**(13), 3165–3166 (2001).
36. A. Mahdjoub and L. Zighed, "New designs for graded refractive index antireflection coatings," Thin Solid Films **478**(1-2), 299–304 (2005).
37. W. H. Southwell, "Gradient-index antireflection coatings," Opt. Lett. **8**(11), 584–586 (1983).
38. F. J. García-Vidal, J. M. Pitarke, and J. B. Pendry, "Effective medium theory of the optical properties of aligned carbon nanotubes," Phys. Rev. Lett. **78**(22), 4289–4292 (1997).
39. J. Gao, R. Chen, D. H. Li, L. Jiang, J. C. Ye, X. C. Ma, X. D. Chen, Q. H. Xiong, H. D. Sun, and T. Wu, "UV light emitting transparent conducting tin-doped indium oxide (ITO) nanowires," Nanotechnology **22**(19), 195706 (2011).

1. Introduction

A technologically import group of materials that exhibit high optical transparency and outstanding electrical conductivity is the transparent conducting oxides (TCOs) [1–4]. Indium tin oxide (ITO) is one of the most frequently investigated TCOs. It has been extensively studied as transparent electrodes in optoelectronic devices, e.g., biosensor [5], optical disk cavities in sub-wavelength size [6], solar cells [7], liquid crystal displays [8, 9], and light emitting diodes (LED) [10]. On the other hand, the performance of material depends on the different nanostructure, such as nanosheets, nanobelts and nanocolumns [11]. Recently, ITO nanocolumns, including nanorods, nanopillars, nanowires and nanowhiskers have been successfully employed to enhance efficiency of photovoltaics and LED, because of their broadband and omnidirectional antireflection (AR) characteristics [12–14]. In particular, ITO nanocolumns exhibit excellent transmittance (>95%) in the visible range [15], and the room-temperature resistivity of individual nanocolumn can be ~100 μΩ·cm to several thousands of μΩ·cm [16]. However, relatively few works on the study of electrical and optical properties of ITO nanocolumns have been reported [15–17]. Conventional Hall measurements require making electrical contacts on the nanostructures and could be destructive. On the other hand, scanning probe measurements can only measure individual nanocolumn instead of providing behavior of carriers over a usable area [16, 17].

Further, it is interesting to explore the application of ITO for the far-infrared electromagnetic wave, in view of the growing demand for terahertz (THz) devices. Indeed, several kinds of ITO devices designed in the THz region, e.g., dichroic mirror [18], micro-strip lines [19], optical modulation in a parallel plate waveguide [20], and metallic wave-impedance matching layers [21], have been demonstrated. As a result, a better understanding of the far-infrared optical and electrical properties of ITO material is essential. In the past decade, both the reflection and transmission Fourier transform infrared spectroscopy (FTIR) methods have been applied to determine the optical and electrical properties of conducting films [22, 23]. Recently, THz time-domain spectroscopy (THz-TDS) has been extensively used for investigating the physical parameters of a wide-range of materials relevant to this work such as bulk semiconductor [24], epilayers [25], thin metal films [26], and a variety of nanostructures [27]. A few groups have reported THz-TDS studies on the electrical and optical properties of the bulk ITO material [23, 28]. To our knowledge, there is no previous work reporting the characteristics of ITO nanocolumns in the THz frequency range. Further, the model of thin film approach with effective medium theory has always been employed to the analysis the nanostructure in the THz frequency range [27]. In this paper, we report an investigation of the frequency-dependent complex conductivities and dielectric characteristics of the bottom layer of ITO nanowhiskers atop the substrate, which layer determines the electrical properties of devices using such nanowhiskers as anti-reflective, conducting electrodes. Consistent results can only be obtained by modeling the ITO nanowhiskers as a graded-refractive-index (GRIN) structure. Key parameters of such as mobility (μ) and carrier concentration (N_e), are extracted by the classical generalization of the Drude formula, also called Drude-Smith model [29].

#165387 - $15.00 USD Received 23 Mar 2012; revised 25 Apr 2012; accepted 30 Apr 2012; published 10 May 2012

2. Preparation and characterization of ITO nanowhiskers

Indium Tin-Oxide (ITO) nanowhiskers were deposited on the (100) oriented silicon substrate with high resistivity using electron-beam evaporation. The double-side-polished silicon substrate was attached to a holder, which was tilted at a deposition angle of 70° with respect to the incident vapor flux. This system was equipped with seven holders which circle around the center of the chamber at a speed of 10 rpm during the deposition. The target source contained 5 wt % SnO_2 and 95 wt % In_2O_3 was placed on the bottom center of the chamber. At the beginning of the evaporation, the chamber pressure was pumped down to ~10^{-6} torr, followed by the introduction of a nitrogen flow rate at 1 sccm to create an oxygen-deficient atmosphere. During growth, the chamber was stabilized at 260 °C and ~10^{-4} torr. Figure 1 shows the scanning electron microscopy (SEM) images of the ITO nanowhiskers with two different deposition times: (a) 16.5 minutes and (b) 22.0 minutes at a titled 45° view. The corresponding cross-sectional images are shown in Figs. 1(c) and 1(d), respectively, where the total heights of nanowhiskers are estimated to be 418 nm and 698 nm. Further, the bottom layers of ITO nanowhiskers could consider as a thin film, and the thickness are decided to be 100 nm and 165 nm by the cross-sectional images. Figure 1(a) shows the formation of ITO nanowhiskers with a diameter of 100 nm at a relatively short deposition time, where the nanowhiskers are randomly distributed on the silicon substrate. Figure 1(b) shows the formation of nanowhiskers, which includes a central trunk and several branches on the sides. As seen at Fig. 1(b), a longer deposition time results in a higher density of whiskers.

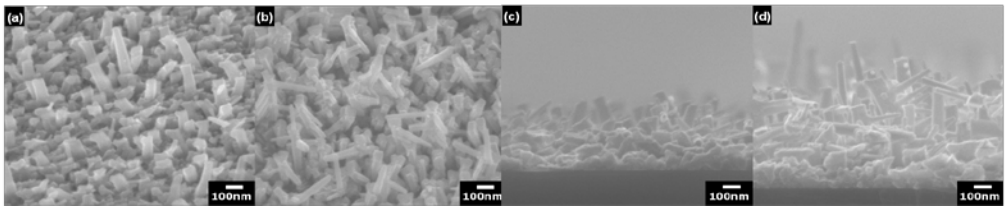

Fig. 1. The scanning electron microscopy images of the ITO nanowhiskers fabricated with different deposition times: (a) 16.5 minutes (b) 22 minutes. The corresponding cross-sectional images in (c) and (d) show an estimated height of 418 nm and 698 nm, respectively.

A UV-vis-NIR spectrophotometer (Hitachi U-4100) with an integrating sphere was used for obtaining the reflectance spectra of the ITO nanowhiskers from the visible to the near-infrared. These are shown in Fig. 2. In the region of 200~2,600 nm, ITO nanowhiskers exhibit broadband AR property. The reflectance is as low as 15%, which are much lower than that of the bare silicon wafer in the same spectral range. The nanowhiskers grown for 16.5 minutes with height of 418 nm exhibit lower reflection in the visible than that in the near-infrared. Similar but distinctive trend are observed for higher-density whiskers grown for 22 minutes (See Fig. 2). For example, the reflectance in the NIR is 5% lower for 698nm-high samples than 418nm-high samples. The reverse is observed in the visible. That is, reflectance can be manipulated somewhat for the NIR and visible spectral range by adjusting the deposition time of ITO nanowhiskers. Similar behaviors have been observed in ITO nanowhiskers grown on micro-grooved silicon surfaces [30]. For such samples, the diameters of trunk and branches are comparable to the visible wavelengths. It is plausible that more substantial scattering in the visible band for the higher-density samples contribute to this observation.

#165387 - $15.00 USD Received 23 Mar 2012; revised 25 Apr 2012; accepted 30 Apr 2012; published 10 May 2012

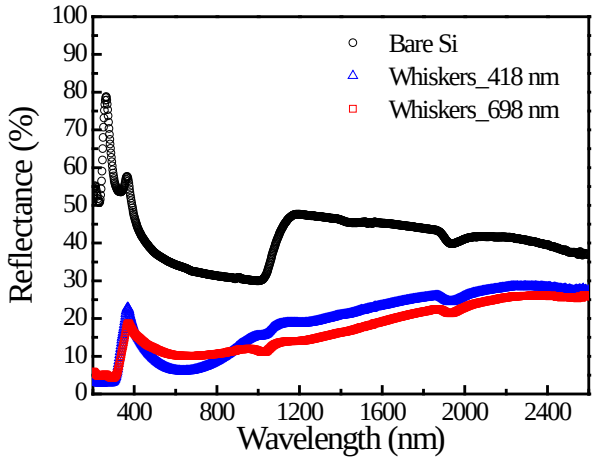

Fig. 2. The reflectance spectra of the bare silicon wafer (black circles) and ITO nanowhiskers with thickness of 418 nm (blue triangles) and 698 nm (red cubes) in the wavelength range of 200~2600 nm.

The transmission electron microscopy (TEM) with a line-scan energy dispersive X-ray (EDX) analysis was employed to characterize the structures of ITO whiskers. As shown in Fig. 3(a), the ITO nanowhiskers structure consists of a trunk and many branches, and the diameters are 100 nm and 50 nm, respectively. The branches grow perpendicularly to the trunk. As seen at Fig. 3(b), the high-resolution TEM image shows the lattice pattern of an ITO trunk. The diffraction pattern reveals the crystalline property, which corresponds to a lattice constant of 5.18 Å. Figure 3(c) displays the line-scan profile of an ITO trunk, where both the In and O compositions vary from the center to the edge due to an integration over different thicknesses of the rod structure. However, the Sn composition shows little variation and the concentration of Sn is less than 1% in the analysis of single point EDX, compared to In and O. The Sn atoms play the role of a catalyst which assists the growth of the ITO nanowhiskers [31, 32]. In these structures, the growth mechanism presumably involves a tin-induced self-catalytic vapor-liquid-solid or vapor-solid process [33–35], which is still under investigation.

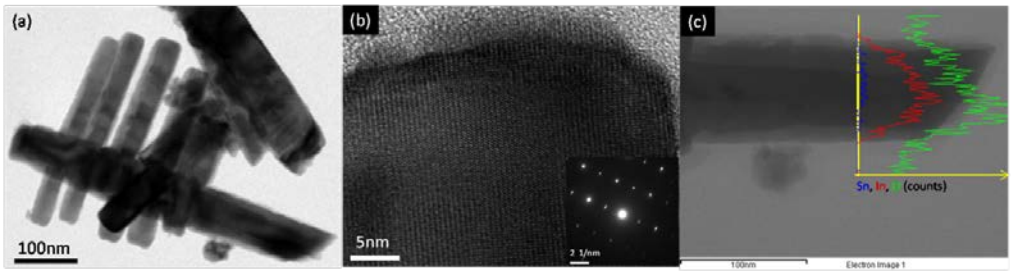

Fig. 3. The TEM characterizations of ITO Nano-whiskers. (a) The TEM images reveal the structures of trunks and branches. (b) The high-resolution image shows the lattice pattern, corresponding to a constant of 5.18Å, and the XRD diffraction pattern of the corresponding crystalline structure (inset). (c) The line-scan profile in an EDX analysis of a ITO trunk. The composition profiles of In and O show significant variation from the edge to center, while the Sn composition show little variation.

The crystalline structure of the ITO nanowhiskers was characterized by X-ray diffraction (XRD) with high resolution. Figure 4 describes the XRD patterns for different thickness of samples. The characteristic pattern of ITO nanowhiskers is almost the same as nanowires [34]. From these patterns, there is almost no amorphous structure, and we can find that the

#165387 - $15.00 USD Received 23 Mar 2012; revised 25 Apr 2012; accepted 30 Apr 2012; published 10 May 2012

ITO nanowhiskers layer have a ⟨111⟩ preferred orientation because the intensity of the (222) peak is stronger than others. The samples with two different deposition times show a similar crystal structures. However, the intensity ratios (222)/(400) are 2.72 and 1.30, respectively. That is, the intensity ratio reduces with increasing the deposition time.

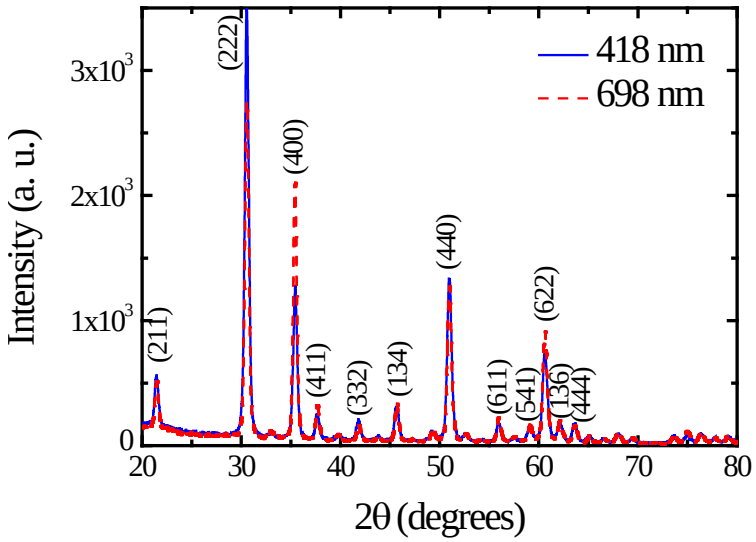

Fig. 4. X-ray diffraction patterns for ITO nanowhiskers deposited on silicon. The blue solid line and red dashed line correspond to ITO nanowhiskers with thicknesses of 418 nm and 698 nm, respectively.

3. Experimental methods

3.1 THz-TDS system

For the THz time-domain measurement, we employed a typical antenna-based THz-TDS which has been described in detail [23]. The femtosecond laser is a mode-locked Ti:Sapphire laser with an average power of ~400 mW at a repetition rate of 82 MHz producing ~35fs. Its central wavelength is 800nm and the bandwidth (full-width-at-half maximum; FWHM) is around 43nm. The power spectral signal-to-noise ratio of THz-TDS system is as high as $10^{6.5}$, and the radius of THz beam waist through ITO nanowhiskers sample is around 4 mm. During the measurement, the system was purged with nitrogen and maintained at a relative humidity of 4.0 ± 0.5%.

3.2 Determination of THz optical constants

In general, the analysis of optical properties of nanostructured materials in the THz frequency treats the medium as a thin film and incorporating the effective medium theory. We were unable to get consistent results for optical constants of ITO nanowhiskers using the approach, however. This is tentatively attributed to the low density of ITO nanowhiskers in our samples, which is not suitable to think as a uniform film. Here, we assume the ITO nanowhiskers with AR characteristics as a kind of GRIN structure. The GRIN structure of the present ITO nanowhiskers with thickness d is shown in Fig. 5, where n_{Air} and n^*_{Sub} represents the refractive indices of air and silicon substrate, respectively. The multilayered model was applied with the relation of $n_{\mathrm{Air}} < n^*_1 < n^*_2 <\ldots< n^*_{\mathrm{m}} <\ldots< n^*_{\mathrm{N}}$. In order to choose the appropriate profile of refractive indices leading to minimum reflectance in the z-direction, the Fermi profile [36, 37], is used and described by the following form:

#165387 - $15.00 USD Received 23 Mar 2012; revised 25 Apr 2012; accepted 30 Apr 2012; published 10 May 2012

$$f_{\mathrm{ITO}}(z) = 1 - \frac{1}{1+e^{b(z-z_0)}}, \tag{1}$$

where b and z_0 are used to describe the form of GRIN profile, and can be determined from the SEM images in Fig. 1. The parameter b is related to the thickness d_1 of the bottom layer of ITO nanowhiskers, and $z_0 = d/2$. Combined with the simple effective medium theorem (EMT) [38], the thickness-dependent refractive indices are defined. Here, each sample of ITO nanowhiskers is subdivided into 200 sections (N = 200).

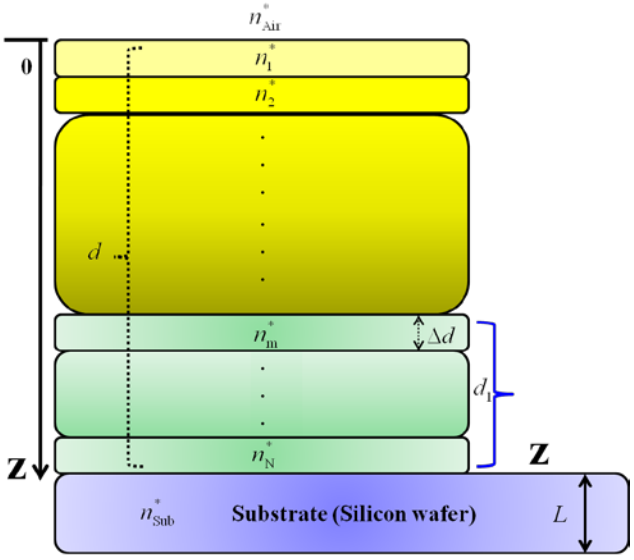

Fig. 5. Sketch of the graded-refractive-index structure of ITO nanowhiskers.

For a monochromatic plane THz wave propagating at normal incidence, we can write the electric field of the THz wave transmitted through the bare silicon substrate as

$$E^*_{\mathrm{Sub}}(\omega) = E^*_0 t^*_{\mathrm{Air,Sub}} t^*_{\mathrm{Sub,Air}} \times \exp\left[i(\omega/c)n_{\mathrm{Air}}d\right]\exp\left[i(\omega/c)n^*_{\mathrm{Sub}}L\right], \tag{2}$$

where $E^*_0(\omega)$ is the electric field of incident THz signal. The ratio $t^*_{\mathrm{Air,Sub}} = 2n_{\mathrm{Air}}/\left(n_{\mathrm{Air}} + n^*_{\mathrm{Sub}}\right)$ and $t^*_{\mathrm{Sub,Air}} = 2n^*_{\mathrm{Sub}}/\left(n^*_{\mathrm{Sub}} + n_{\mathrm{Air}}\right)$ are the transmission coefficients of the THz signal from air to the bare silicon substrate and from the substrate to the air, respectively; $n_{\mathrm{Air}}(\omega)$ and $n^*_{\mathrm{Sub}}(\omega)$ are the complex refractive indices of the air and substrate, respectively; ω, and c are the angular frequency and speed of light, respectively. Similarly, the electric field of the THz wave passed through the sample of ITO whiskers can be written as

$$\begin{aligned} E^*_{\mathrm{ITO}}(\omega) = {} & E^*_0 t^*_{\mathrm{Air},1} t^*_{12} t^*_{23} \ldots t^*_{(\mathrm{m}-1)\mathrm{m}} \ldots t^*_{\mathrm{N,Sub}} \\ & \times \exp\left[i(\omega/c)(n^*_1 + n^*_2 + n^*_3 \ldots + n^*_{\mathrm{m}-1} + n^*_{\mathrm{m}} + \ldots n^*_{\mathrm{N}})(d/\mathrm{N})\right] \\ & \times t^*_{\mathrm{Sub,Air}} \times \exp\left[i(\omega/c)n^*_{\mathrm{Sub}}L\right], \end{aligned} \tag{3}$$

where $t^*_{\mathrm{Air},1} = 2n_{\mathrm{Air}}/\left(n_{\mathrm{Air}} + n^*_1\right)$, $t^*_{(\mathrm{m}-1),\mathrm{m}} = 2n^*_{(\mathrm{m}-1)}/\left(n^*_{(\mathrm{m}-1)} + n^*_{\mathrm{m}}\right)$ and $t^*_{\mathrm{N,Sub}} = 2n^*_{\mathrm{N}}/\left(n^*_{\mathrm{N}} + n^*_{\mathrm{Sub}}\right)$ are the transmission coefficients from the air to the 1st layer of sample, from the (m−1)th layer to the mth layer of the sample and from the Nth layer of the sample to the substrate,

#165387 - $15.00 USD Received 23 Mar 2012; revised 25 Apr 2012; accepted 30 Apr 2012; published 10 May 2012

respectively; $n_1^*(\omega)$, $n_2^*(\omega)$, $n_3^*(\omega)$, $n_{m-1}^*(\omega)$, $n_m^*(\omega)$ and $n_N^*(\omega)$ are the complex refractive indices of different layers of the GRIN structure. For extracting the optical constants, the theoretical transmittance of THz field can be written as

$$T_{\text{Theo}}^*(\omega) = E_{\text{ITO}}^*(\omega)/E_{\text{Sub}}^*(\omega) = t_{\text{Air},1}^* t_{12}^* t_{23}^* \ldots t_{(m-1)m}^* \ldots t_{\text{N,Sub}}^* \times \exp\left[i(\omega/c)(d/\text{N})(n_1^* + n_2^* + n_3^* + \ldots + n_{(m-1)}^* + n_m^* + \ldots + n_N^* - \text{N}\cdot n_{\text{Air}}^*) \right] / t_{\text{Air,Sub}}^*. \quad (4)$$

Experimentally, the transmittance $T_{\text{Exp}}^*(\omega)$ is determined from the ratio of the transmitted THz spectra through both the bare substrate and the sample of ITO nanowhiskers. Finally, by finding the minimum of error function of $T_{\text{Theo}}^*(\omega)$ and $T_{\text{Exp}}^*(\omega)$, the complex refractive indices n_N^* ($n_N^* = n + i\kappa$) can be extracted.

3.3 THz conductivity and Drude-Smith model approach

The complex conductivity (σ^*) of the material under study can be written as,

$$\left(n_N^*\right)^2 = \varepsilon^*(\omega) = \varepsilon_\infty + i\frac{\sigma^*(\omega)}{\omega\varepsilon_0}, \quad (5)$$

where ε^* is the complex dielectric constant; ε_∞ = 4 [23], is the high-frequency dielectric constant contributed by the bound electrons; ε_0 = 8.854 × 10^{-12} (F/m) is the free-space permittivity.

In order to describe the THz conductivity in the nanomaterial, the Drude-Smith model is applied to fit the experimentally deduced conductivity [27, 29]. In this model,

$$\sigma^*(\omega) = \frac{\varepsilon_0\omega_p^2\tau}{1 - i\omega\tau}\left(1 + \frac{\gamma}{1 - i\omega\tau}\right), \quad (6)$$

where ω_p and τ are the plasma frequency and the carrier scattering time, respectively; the parameter γ is the expectation value of cosine of scattering angle or the persistence of velocity. The value of γ can vary from 0 (isotropic scattering or Drude-like carriers) to –1 (full carrier backscattering or fully localized carriers). The parameters ω_p and τ can be extracted by fitting the experimentally deduced conductivity with the Drude-Smith model. Further, the parameters N_e and μ can also be determined from the relations $N_e = \varepsilon_0\omega_p^2 m^*/e^2$ and $\mu = (1 + \gamma)\cdot e\tau/m^*$, respectively, where $m^* = 0.3m_0$ [39], is the electron effective mass; m_e = 9.109 × 10^{-12} kg, is the electron's mass; e = 1.602 × 10^{-19} C, is the electron charge.

4. Results and discussions

The frequency-dependent complex refractive indices and power absorption of ITO nanowhiskers with different thicknesses (418 nm and 698 nm) are shown in Fig. 6. Here, we only show the values of n_N^* ($n + i\kappa$) for the bottom layer of whiskers structure. The complex refractive indices of every layer in the nanowhiskers can be obtained through the Fermi profile. The real parts of refractive indices (n) of the ITO nanowhiskers with different thicknesses are very similar to each other, decreasing almost linearly from 68 to 40 in the 0.2~2.0 THz frequency range. Below 0.9 THz, the real index, n of the bottom layer of taller nanowhiskers, shown in Fig. 6(a), are always larger than shorter ones, and the difference between them is reduced at higher frequencies. On the other hand, the imaginary part of refractive indices, κ (see the inset of Fig. 6(b)), varies from 10 to 30 in the 0.2~2.0 THz

#165387 - $15.00 USD Received 23 Mar 2012; revised 25 Apr 2012; accepted 30 Apr 2012; published 10 May 2012

frequency range, with the taller nanowhiskers. It can be seen that the absorption coefficients increase with frequency. No apparent absorption peaks are observed below 2.0 THz.

The experimental and theoretical complex conductivities ($\sigma^* = \mathrm{Re}\{\sigma\} + i\mathrm{Im}\{\sigma\}$) of the bottom layer of ITO nanowhiskers with different heights are shown in Fig. 7. The $\mathrm{Re}\{\sigma\}$ increases slowly as the frequency increased; the imaginary part of conductivity $\mathrm{Im}\{\sigma\}$ reaches a minimum value around 1.0 THz, and is always negative in the 0.2~2.0 THz. Both $\mathrm{Re}\{\sigma\}$ and $\mathrm{Im}\{\sigma\}$ are fitted well by the Drude-Smith Model. For whiskers with different heights (418 and 698 nm), ω_p are in the range of 864~920 rad·THz, and τ is in the range of 60~69 fs. The variation of carrier scattering times is small. This indicates that the grain sizes of the samples are almost the same. The XRD results shown in Fig. 4, which show the similar full width at half maximum of the intensity of the (222) peak, correlate well with the deduced scattering times. Besides, the relatively longer carrier scattering times in the bottom layers of ITO nanowhiskers also indicate its crystallinity.

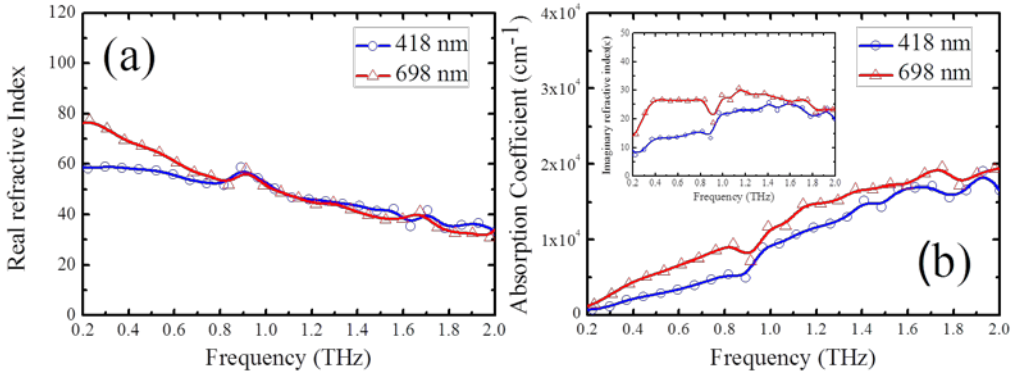

Fig. 6. (a) The real parts of the refractive indices of ITO nanowhiskers with thickness of 418 nm (blue circles) and 698 nm (red triangles). (b) The power absorption of ITO nanowhiskers with thickness of 418 nm (blue circles) and 698 nm (red triangles). The imaginary parts of the refractive indices of ITO nanowhiskers with thickness of 418 nm (blue circles) and 698 nm (red triangles) are shown in the inset.

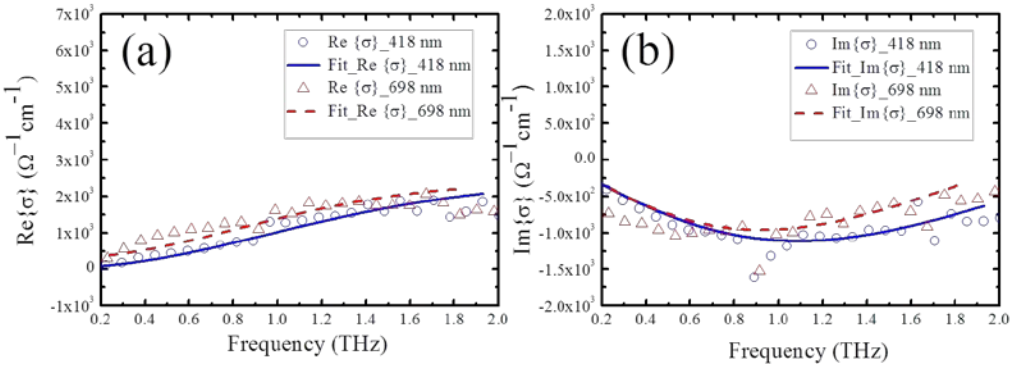

Fig. 7. (a) The real parts of conductivities of ITO nanowhiskers with thickness of 418 nm (blue circles) and 698 nm (red triangles). (b) The imaginary parts of the conductivities of ITO nanowhiskers with thickness of 418 nm (blue circles) and 698 nm (red triangles). The blue solid lines and red dashed lines are the corresponding fitting results based on the Drude-Smith model.

The mobility and carrier concentrations, μ and N_e of the above ITO whiskers are determined to be 2~26 $\mathrm{cm^2V^{-1}s^{-1}}$ and 7~8 × 10^{19} $\mathrm{cm^{-3}}$, respectively. The value of γ is around −0.96, corresponding to strong backscattering and localization of carriers in the bottom layer of ITO nanowhiskers. Since DC conductivity in the Drude-Smith model is given by $\varepsilon_0\omega_p^2\tau\cdot(1$

#165387 - $15.00 USD Received 23 Mar 2012; revised 25 Apr 2012; accepted 30 Apr 2012; published 10 May 2012

+ γ), the large negative value of γ means backscattering and fully localized carriers occur at the boundaries of nanowhiskers. As a result, the DC conductivity 418nm- and 698nm-high ITO nanowhiskers are 27 $\Omega^{-1}cm^{-1}$ and 289 $\Omega^{-1}cm^{-1}$, respectively.

In the following, we examine the possible mechanisms for the observation of a minimum in the imaginary component of conductivity of the indium-tin-oxide nanowhiskers (see Fig. 7(b)). First of all, we rewrite Eq. (6), into its real and imaginary parts, i.e., Re{σ} and Im{σ}:

$$\mathrm{Re}\{\sigma\} = \frac{\varepsilon_0 \omega_p^2 \tau \left[(1+\gamma) + \omega^2 \tau^2 (1-\gamma) \right]}{\left(1+\omega^2\tau^2\right)^2}, \tag{7}$$

$$\mathrm{Im}\{\sigma\} = \frac{\varepsilon_0 \omega \omega_p^2 \tau^2 \left(1+2\gamma+\omega^2\tau^2\right)}{\left(1+\omega^2\tau^2\right)^2}. \tag{8}$$

Since γ is in the range of –0.5~–1.0, there are one maximum of Re{σ}, one maximum and one minimum of Im{σ}. In addition, for Im{σ}, the minimum is always lower than the maximum in frequency. Taking the derivative of Eq. (7), we expect a maximum value of Re{σ} located at the angular frequency of $\omega_{\mathrm{Re,\ Max}}$, = $[-(1 + 3\gamma)/(1-\gamma)]^{1/2}/\tau$. Similarly, the extreme values of Im{σ} should exist at the angular frequencies of $\omega_{\mathrm{Im,Max}}$, = $[-3\gamma + (9c^2 + 2c + 1)^{1/2}]^{1/2}/\tau$, and $\omega_{\mathrm{Im,Min}}$, = $[-3\gamma-(9c^2 + 2c + 1)^{1/2}]^{1/2}/\tau$, respectively. Here, extreme values of Re{σ} and Im{σ} are functions of the carrier scattering time (τ) and the expectation value of cosine of scattering angle (γ). Therefore, the observed behaviors of $\omega_{\mathrm{Re,\ Max}}$, $\omega_{\mathrm{Im,Max}}$ and $\omega_{\mathrm{Im,Min}}$ reflect the characteristics of long scattering times and strong backscattering of ITO nanowhiskers. For 418nm-high whiskers, $\omega_{\mathrm{Re,\ Max}}$, $\omega_{\mathrm{Im,Max}}$ and $\omega_{\mathrm{Im,Min}}$ are estimated to be near 2.6 THz, 6.3 THz and 1.1 THz, respectively. Simialarly for 698nm-high whiskers, $\omega_{\mathrm{Re,\ Max}}$, $\omega_{\mathrm{Im,Max}}$ and $\omega_{\mathrm{Im,Min}}$ are estimated to be near 2.2 THz, 5.4 THz and 0.9 THz, respectively. Since the reliable frequency range of our THz-TDS system is 0.2~2.0 THz, we can only observe the minimum of Im{σ} ($\omega_{\mathrm{Im,Min}}$), which is around 1.0 THz for the two samples of ITO nanowhiskers.

In Comparison, μ and N_e of ITO thin films [23] are around 30~40 $cm^2V^{-1}s^{-1}$ and 2~5 × 10^{20} cm^{-3}, respectively. However, ITO nanowhiskers exhibit longer carrier scattering times (~65 fs) than that of ITO thin films (~7 fs). This is attributed to the effect of long-range transport related to γ. The value of γ which is around –0.96 for the ITO nanowhiskers will reduce the mobility of such samples, because the dependence of DC mobility on the factor of $1 + \gamma$. That is, the carriers in the bottom layer of ITO nanowhiskers can have long carrier scattering times due to its large grain size. On the other hand, its mobility is lower due to the part of carriers with long-range transport between the connected grains. We note that, the mobility of the samples will vary, depending on the growth conditions and material structures, as in Zinc oxide (ZnO) [27]. As found in this work, the ZnO nanowires also have the persistence of velocity factor very close to –1, γ ~–0.92. Besides, the mobilities of ZnO nanowires (~16 $cm^2V^{-1}s^{-1}$) were also found to be lower than those of the thin films (~40 $cm^2V^{-1}s^{-1}$) [27].

5. Conclusions

Indium-tin-oxide (ITO) nanowhiskers with attractive electrical and anti-reflection properties were prepared by the glancing-angle electron-beam evaporation technique. Structural and crystalline properties of such nanostructures were examined by scanning transmission electron microscopy and X-ray diffraction. Their frequency-dependent complex conductivities, refractive indices and absorption coefficients have been characterized with terahertz time-domain spectroscopy (THz-TDS), in which the nanowhiskers were considered as a graded-refractive-index (GRIN) structure instead of the usual thin film model. The electrical properties of ITO GRIN structures are analyzed and fitted well with Drude-Smith

#165387 - $15.00 USD Received 23 Mar 2012; revised 25 Apr 2012; accepted 30 Apr 2012; published 10 May 2012

model in the 0.2~2.0 THz band. For nanowhiskers 418nm and 698nm in heights, the plasma frequencies are 864 versus 920 rad·THz, and carrier scattering time are 60 versus 69 fs, respectively. The carrier mobility, carrier concentration are also determined to be 2 versus 26 $cm^2V^{-1}s^{-1}$, 7 versus 8 × 10^{19} cm^{-3}, respectively. Our results indicate that the ITO nanowhiskers and its bottom layer atop the substrate exhibit longer carrier scattering times than ITO thin films. This signifies that ITO nanowhiskers have an excellent crystallinity with large grain size, consistent with X-ray data. Besides, the expectation value of cosine of scattering angle is ($\gamma \sim -0.96$). This indicates a strong backscattering effect and fully carrier localization in the ITO nanowhiskers. Thus ITO nanowhiskers are attractive for THz device applications, in additional to its broad interests for the visible spectral range.

Acknowledgments

This works was supported by a grant of the National Science Council 99-2120-M-006-002 and the Academic Top University Program of the Ministry of Education. The authors would like to thank Professor Hao-Chung Kuo for use of the electron-beam evaporator. They would also like to than Prof. Tsing-Hua Her for many useful discussions.

#165387 - $15.00 USD Received 23 Mar 2012; revised 25 Apr 2012; accepted 30 Apr 2012; published 10 May 2012